Ab-initio study of the ground and low-lying excited states including the spin-orbit effect of RbBa molecule and laser cooling feasibility

Hela Ladjimi, Wissem Zrafi, Abdul-Rahman Allouche, Hamid Berriche

Ab-initio study of the ground and low-lying excited states including the Spin-Orbit effect of RbBa molecule and laser cooling feasibility

Hela Ladjimi[1,2,a], Wissem Zrafi[1], Abdul-Rahman Allouche[2], Hamid Berriche[1,3,b]

[1]Laboratory of Interfaces and Advanced Materials, Faculty of Science, University of Monastir, 5019 Monastir, Tunisia.
[2]Institut Lumière Matière, UMR5306 Université Lyon 1-CNRS,Université de Lyon, 69622 Villeurbanne Cedex, France.
[3]Department of Mathematics and Natural Sciences, School of Arts and Sciences, American University of Ras Al Khaimah, RAK, P.O. Box 10021, UAE.

[a]helaladjimi91@gmail.com,[b]hamid.berriche@aurak.ac.ae

ABSTRACT:

In this work, we present a thorough theoretical structure and spectroscopic study of the ground and low lying excited states of RbBa molecule. High-level *ab-initio* calculations are performed, using MCSCF/MRCI+Q level of method, based on the effective core potential (ECP) and core-polarization potential (CPP) approach. The potential energy curves, spectroscopic parameters, vibrationnel energy levels of the 16($^{2,4}\Sigma^+$,$^{2,4}\Pi$,$^{2,4}\Delta$) first electronic states, with respect to the lowest five dissociation limits were calculated. The comparison of the spectroscopic constants of the ground state $X^2\Sigma^+$ with the available theoretical work, are in good agreement. The study of all the excited states is performed in this work for the first time. Afterwards, the spin-orbit operator is incorporated in valence MRCI calculation using optimized relativistic spin-orbit pseudo-potentials and 33 Ω states are generated and split into Λ-S states. In addition, both relativistic and non relativistic calculations of permanent and transition dipole moments are presented and discussed. Stimulated black body (T =300 K) and spontaneous transition rates of vibrational states of $X^2\Sigma^+$ state were evaluated. The related vibrational lifetimes for RbBa are found to be in order of 10^3 second which is sufficiently large for ultracold experiments. Moreover, the vibrational life-time for the $A^2\Sigma^+(v')$ and $A^2\Pi$ (v'') states are measured and the possibility of Laser Cooling for the RbBa molecule is discussed based on *Franck–Condon* factors calculation of $A^2\Sigma^+$ (v')→ $X^2\Sigma^+(v)$ and $A^2\Pi(v'')$ → $X^2\Sigma^+(v)$ transition. This work represents a significant contribution for experimentalists as it provides efficient information in order to form cold alkali and alkaline-earth RbBa molecules.

Keywords: Ab-initio calculation; Electronic structure; Dipole moments; Spin-orbit coupling; Franck–Condon factors; laser cooling.

1. INTRODUCTION

In recent years, mixed diatomic molecules composed with one alkali-metal atom and one alkaline-earth atom became particularly interesting for the community of chemical physicists especially in the field of cold and ultracold molecular physics. These types of dipolar molecule possess a strong permanent dipole moment in combination with a magnetic dipole moment in their ground state $^2\Sigma^+$ and they exhibit a non-zero electronic spin angular momentum in their rovibrational ground state**[1, 2, 3]**.These properties enable many exciting applications and experiments, such as Feshbach resonances **[4]**,precise measurements of fundamental physical constants with high resolution spectroscopy **[5, 6]**, realization of quantum simulations**[7]**, topological quantum phases and simulations of spin models in optical lattices **[8-9]** , which were mediated by the induced electric dipole-dipole interaction. A theoretical calculation of the molecular electronic structure is necessary to understand the mechanisms of the production of cold and ultracold molecules such as: collisional cooling and the lasers required for the cooling experiments. Also, the estimations of the permanent and transition dipole moment (PDM), black body radiative lifetime and Franck-condon factor are important in the study of interactions between ultracold molecules. This information leads to valuable insights into the stability of a Bose-Einstein condensate and the Fermi degeneracy in a single quantum state **[10]**.

Experimentally, the Rb-Alkaline-earth molecules, as RbCa **[11]**, RbSr **[7, 12, 13, 14]** are found to be suitable candidates for the preparation of ultracold ground state molecules. Theoretically, the neutral Rb-AKE molecules have been extensively studied in many works, such as RbBe**[15]**, RbMg **[16]**, RbCa **[11, 17]**, RbSr**[18, 19]**. RbBa represents another interesting molecule, because Rb and Ba are well under control in ultracold atomic physics. Furthermore, ultracold Rb_2 ground state molecules **[20]** as well as Bose-Einstein condensates of Rb**[21]** have been experimentally achieved.

Compared with systematic researches on other systems of the Alkali-Alkaline-earth diatomic, RbBa has not been well studied and data for this molecular system remain unavailable. Only a theoretical calculation was carried out by Gou et al **[22]** where only the ground potential energy curves (PECs) and dipole moment functions are exhibited. The computations, performed at the CASSCF and MRCI level with the small-core scalar relativistic effective core potentials ECP28MDF for Rb and ECP46MDF for Ba deduced molecular constants of 9.31Bohr and 1471 cm^{-1} for R_e and D_e respectively. Therefore, it is necessary to provide an accurate analysis of the excited electronic states of the RbBa

molecule which can be an initial step for the production of this molecule by photoassociation. For that we present, in this paper, an extensive theoretical study for the RbBa molecule based on the CPP approach: Potential energy curves (PECs) and permanent dipole moments (PDMs) for the ground $X^2\Sigma^+$ (defined also as (1) $^2\Sigma^+$) and several low-lying electronic states $^{2,4}\Sigma^+$, $^{2,4}\Pi$ and $^{2,4}\Delta$ correlated into the first five dissociation limits. The corresponding spectroscopic constants have been calculated for all bound states. The allowed transition dipole moments (TDMs) have been also investigated between all calculated states. To verify the accuracy of the TDM, we compared our calculations at large distance (atomic limit) with the available published atomic TDMs. Also, based on the relativistic pseudopotential method, the spin-orbit coupling was introduced and 33 Ω states are generated. The effect of the spin-orbit splitting on the potential energy curves and the dipole moment was detected. In addition, the vibrational energy levels, black body (T =300 K), spontaneous transition rates and the radiative lifetimes of the vibrational states of the ground state $X^2\Sigma^+$ were calculated. Moreover, the vibrational lifetime for the $A^2\Sigma^+$ (v') and $A^2\Pi(v'')$ are considered and the possibility of the feasibility of Laser Cooling for RbBa molecule is also discussed based on *Franck–Condon* factors calculation of $A^2\Sigma^+$ (v')→ $X^2\Sigma^+$ (v) and $A^2\Pi(v'')$ → $X^2\Sigma^+$ (v) transition.

This paper is organized as follows: In **Section 2**, we briefly present theoretical and computational method and give numerical details. **Section 3** is devoted to the presentation of our various results. Finally, we present our conclusions in **Section 4**.

2. THEORETICAL ASPECTS

The present calculation is based on complete active space self-consistent field CASSCF+ multi-reference configuration interaction MRCI methods and ECP+CPP approach which rely on the modeling of the Rb^+ and Ba^{2+} closed-shell cores by an effective core potential (ECP) completed by a core-polarization potential (CPP). A state-averaged CASSCF calculation is carried out before MRCI to generate the reference molecular orbitals. Over three thousand CSFs are involved for each state. The Davidson correction, noted as MRCI+Q, was then invoked in order to account for unlinked quadruple clusters and to correct for higher-order CI terms. All calculations are obtained using the computational chemistry MOLPRO package **[23]**. In this work, we used the effective core potentials SBKJC ECP54 for Ba and SBKJC ECP36 for Rb**[24]**. Subsequently, the RbBa molecule is modeled as an effective three-electron system. The polarization effects of cores are taken into account by an effective Core

Polarization Potential (CPP) according to the formalism proposed by Müller, Flesch, and Meyer **[25]**. The polarizability of the Rubidium and Barium cores are 9.096 a.u. **[26]** and 10.3a.u. **[27]**, respectively. To reproduce the atomic experimental spectra **[27]** of Ba and Rb atoms, the exponential parameter of the cutoff-function and the basis sets were determined by adjusting their parameters and the two resulting atomic Gaussian basis sets are composed of (6s 8p 5d 3f / 6s 8p 4d 3f) and (8s, 8p, 5d, 3f) for Ba and Rb respectively. The corresponding exponential coefficient obtained of the Gaussian type orbitals for the Rb atom are represented in the **Supplementary material (S. TABLE 1)**. The Ba atom basis set was presented in our previous spectroscopic study of the BaCs system **[28]**. The exponential parameters of the cutoff-function are 0.27 $Bohr^{-2}$and 0.3185 $Bohr^{-2}$for Rb and Ba respectively. In addition, at small internuclear separation, the energies of the core-core Ba^{++} and Rb^{+} repulsion is considerable. The calculations are carried out in the C_{2v} symmetry. In the C_{2v} point group, all molecular orbitals MOs are labeled by their symmetries (a_1, b_1, b_2, a_2), and the electronic states are labeled by their symmetries (A_1, B_1, B_2, A_2) too. When the symmetry is reduced from $C_{\infty v}$ to C_{2v}, the correlating relationships are $\sigma \rightarrow a_1$, $\pi \rightarrow (b_1, b_2)$, $\delta \rightarrow (a_1, a_2)$ and $\Sigma^+ \rightarrow A_1$, $\Pi \rightarrow B_1+B_2$, $\Delta \rightarrow A_1+A_2$, $\Sigma^- \rightarrow A_2$. In the CASSCF and MRCI+Q calculations of the RbBa molecule, the active space consists of three electrons and thirty molecular orbitals $14a_1$, $6b_1$, $6b_2$, $4a_2$ (14 6 6 4), refers to as CAS (3, 30). Afterwards, a second type of calculations is also performed including the spin-orbit relativistic effects through the inclusion of effective core potentials (ECP) in the expression of the molecular Hamiltonian. The spin-orbit interaction couples the orbital angular momentum Λ with the spin angular momentum S through its projection Σ on the internuclear axis. This produces a total angular momentum along the internuclear axis $\Omega = |\Lambda \pm \Sigma|$ and characterizes the spin-orbit electronic states. In this approach, spin-orbit states with a well-defined quantum number Ω = 1/2, 3/2, 5/2, 7/2 may arise from the spin-orbit splitting in the parent $^{2,4}\Sigma^{\pm}$, $^{2,4}\Pi$, and $^{2,4}\Delta$ electronic states. The scalar-relativistic effects are taken into account in the pseudopotentials (ECPs) using the Molpro package [23] where the coefficient of the relativistic spin-orbit pseudopotential are optimized and adjusted in order to predict the experimental spin-orbit atomic states [27] for both Ba and Rb atoms. The fitted coefficients are found to be c_p=1.6353444739 and 0.4556898932, c_d=0.2941076339 and -0.0065953068 for Ba atom and c_p = 0.0987768811377494 and 0.216736020700025, c_d = -0.000560258776047519, 0.003616223047858823 and -0.00339511755209459 for Rb atom. The obtained transition energies for atomic states with and without spin-orbit coupling of both Rb and Ba atoms are represented in **Table 1** compared to the experimental results **[27]**. The atomic energy levels of

Rb are well reproduced and a deviation of less than 1.22% is obtained for Ba. In **Table 2**, we reported the molecular asymptotic limits for the first five low lying states compared with experimental ones **[27]** and the corresponding doublet and quartet states. Based on the methods and theories mentioned before, the potential energy curves, permanent and transition dipole moment curves of the low lying electronic states of RbBa molecule in both Λ-S and Ω representations has been calculated as a function of the internuclear distance R. The spectroscopic constants are extracted from the *ab-initio* points interpolated using the least-squares spline method. Both permanent and transition dipole moments are evaluated as an expectation values of the dipole operator with the calculated electronic wave functions. The time-independent Schrodinger equation for the nuclear motion is solved based on the renormalized Numerov algorithm **[29]** and the vibrational lifetimes τ_i of the ground state $X^1\Sigma^+$ was calculated as:

$$\tau_i^{-1} = \sum_{f<i} A_{if} + \sum_f B_{if} \qquad (1)$$

The first term A_{if} is the Einstein coefficient describing the probability of spontaneous emission from the vibrational state *i* to the lower energy state *f*:

$$A_{if} = \frac{4\omega_{if}^3}{3C^3} |\langle i|\mu(R))|f\rangle|^2 \qquad (2)$$

$\omega_{if} = |E_f - E_i|$ is the transition frequency between the two bound states *i* and *f*, and $\mu(R)$ is the permanent dipole moment of the ground state $X^1\Sigma^+$.

The second term is related to the Black Body Radiation (BBR), which is stemming from the surrounding environment at T = 300 K, and it can induce stimulated absorption and emission processes, which are described by the Einstein coefficient $B_{if} = A_{if}N(\omega_{if})$, where the number of black body photons is given by:

$$N(\omega_{if}) = (\exp\left(\frac{\omega_{if}}{k_B T}\right) - 1)^{-1} \qquad (3)$$

The calculation of the vibrational lifetimes of the excited states takes into account two possible transitions: *bound-bound* and *bound-free* transitions. The radiative lifetime of a vibrational level υ' corresponding to the *bound-bound* transitions is given by:

$$\tau_{v'} = \frac{1}{\Gamma_{v'}}, \quad \Gamma_{v'} = \sum_{v=0}^{nvt} A_{vv'} \qquad (4)$$

$A_{vv'}$ is the Einstein coefficient taking for example the transition between $A^2\Sigma^+(v')$ and $X^2\Sigma^+(v)$ levels states. The *bound-free* contribution is calculated using the Franck-Condon approximation proposed by Zemke et al. **[30]**:

$$A_{v'}(bound-free) = \frac{64\pi^2}{3h^4c^3}|\mu(R_{v'+})|^2 FC_{v',cont}(\Delta E)^3_{v',cont} \quad (5)$$

Where $\Delta E_{v',cont} = E_{v'} - E_{as}$ is the energy difference between the vibrational level v' and the energy of the asymptotic limit of the lower electronic state, to which belongs the continuum. The quantity $\mu(R_{v'+})$ corresponds to the transition dipole moment at the right external turning point of the vibrational level *v'*.

$$FC_{v',cont} = \int|\langle\chi_{v'}|\chi_E\rangle|^2 dE = 1 - \sum_{v=0}^{nvt}|\langle\chi_{v'}|\chi_v\rangle|^2 \quad (6)$$

3. RESULTS AND DISCUSSION

3.1 Potential Energy curves

The potential energy curves for 16 low-lying doublet and quartet electronic states: 11 doublet electronic states (five $^2\Sigma^+$, four $^2\Pi$ and two $^2\Delta$) and 5 quartets electronic states (two $^4\Sigma^+$, two $^4\Pi$ and one $^4\Delta$) are calculated using CASSCF and MRCI theory including the Davidson correction. They are correlated to the five lowest asymptotes and calculated for a dense grid, which varies from 6.0 to 30.0 Bohr with a step of 0.1. **Figure 1**, presents the resulting potential energy curves for all states in $^{2,4}\Sigma^+$, $^{2,4}\Pi$ and $^{2,4}\Delta$ symmetries as a function of internuclear distance R. Generally, the shapes of the potential energy curves of the bound states are formed with three parts. Firstly, a repulsive branch at very small internuclear distance where the two atoms brought close to each other and the electronic clouds surrounding the atoms start to overlap. Indeed, in this region the Pauli Exclusion Principle correlates the repulsion between the two atoms and the energy of the system increases abruptly. Then, an attractive part is presented at small and intermediate internuclear distance where the potential energy curves for different states are present with simple wells more or less deep. The origin of the attractive part depends on the particular type of bonding and the depth of the potential energy curve indicates the strength of the bond. Finally, the potential energy starts to be independent, at large internuclear distance, and reaches a constant value indicating the dissociation limits, which is equal to the sum of atomic energies. As showing in **Figure 1**, the potential energy curve for the ground state $X^2\Sigma^+$ is widely separated from the highly excited states. However, the higher excited states are close to each other and interact

much more with the presence of barrier potential. These interactions and behaviors are manifested by the presence of avoided crossings between neighboring states of same symmetry and some crossings between states of different symmetry. Such crossings or avoided crossings, can dramatically alter the stability of molecules owing the possibility of crossing from one state to another and their presence can be important to study non-adiabatic transitions **[31]**.Thus, the positions of avoided crossings between different electronic states of RbBa molecule are reported in **Table 3** where R_{AC} is the internuclear distance at which the avoided crossing occurs and D_E is the energy gap separation.

3.2 Spectroscopic parameters

The spectroscopic constants have been extracted from the PECs for $^{2,4}\Sigma$, $^{2,4}\Pi$ and $^{2,4}\Delta$ symmetries: equilibrium distance R_e, well depth D_e, electronic excitation energy T_e, harmonic frequency ω_e, anharmonic constant $\omega_e x_e$, and rotational constant B_e. These constants were determined by the least-squares interpolation method. The Numerov algorithm was used to determine the nuclear wave function for diatomic molecules. The spectroscopic constants are collected in **Table 4**. The ground state $X^2\Sigma^+$ of RbBa system correlates at large distances to the atomic ground states Ba (^{1}S) and Rb (^{2}S) atoms. It is well separated from the highest states in the same symmetry and shows a unique minimum at 8.75 Bohr and a relatively large depth of well with a value of 1566 cm^{-1}. For this molecule, only the ground state $X^2\Sigma^+$ has been calculated by Gou et al. **[22]**, using of CASSCF and MRCI methods with the small-core scalar relativistic effective core potentials ECP28MDF for Rb and ECP46MDF for Ba **[24]**.The depth of well obtained by the calculation of Gou et al.**[22]** is about 95 cm^{-1} smaller than the present results. The comparison shows that the different method and basis sets used effect more obviously the R_e than the D_e and the difference between the two calculations is about 0.56 Bohr with a relative difference about 6.4%. Our ω_e=42.59 cm^{-1} is in good agreement with that of Gou et al **[22]** ω_e =39.23 cm^{-1}. The two anharmonic frequencies $\omega_e\chi_e$ are also very close to each other. Unfortunately, no experimental data can be found for the considered state. The second covalent asymptote comes from the combination of the Ba(^{3}D) first atomic excited state and Rb(^{2}S) atomic ground state correlates with six molecular states $(2)^2\Sigma^+$, $(1)^4\Sigma^+$,$(1)\ ^{2,4}\Pi$ and $(1)^{2,4}\Delta$. These states are found to be very attractive and possess large depth of wells. We note that the first excited doubled state $(1)^2\Pi$ is the most strongly bound. It possesses, at the equilibrium distance R_e = 7.37 Bohr, the deepest well (D_e = 7825 cm^{-1}) compared to the ground state or remaining excited states for diverse symmetries. The first

doubled $1^2\Delta$ state possesses also a very deep well (D_e = 5086 cm^{-1}) at the equilibrium distance R_e=7.89 Bohr. The combination between second excited state Ba(^{1}D) and ground state Rb(^{2}S) leads to the third dissociation limit that correlates with $(3)^2\Sigma^+$, $(2)^2\Pi$ and $(2)^2\Delta$ molecular states. The $(3)^2\Sigma^+$ and $(2)^2\Pi$ states are founded with unique deep wells of D_e = 4908 and 6273 cm^{-1} respectively. The second state of the delta symmetry $(2)^2\Delta$ is weakly bound with a small attractive well and its D_e does not exceed 897 cm^{-1}. The fourth dissociation limit comes from a combination of the Ba(^{1}S) ground state and Rb(^{2}P) first excited state correlated to the $(4)^2\Sigma^+$ and $(3)^2\Pi$ states. These two states were characterized with unique depth of well at R=9.00 and 8.72 Bohr with depths values D_e = 4986 and 2786 cm^{-1}respectively for $(4)^2\Sigma^+$, $(3)^2\Pi$ states. The combination between the Ba(^{3}P) third excited state and the Rb(^{2}S) ground state generates the fifth dissociation limit and correlates with $(5)^2\Sigma^+$,$(2)\ ^4\Sigma^+$, $(4)^2\Pi$ and $(2)^4\Pi$ state, which are present with simple wells with different depths.

3.3 Spin-Orbit coupling effects on the potential energy

Our molecule is composed of heavy atoms which gives rise to a significant contribution of relativistic effects and consequently influences the electronic properties of RbBa molecules. In this section, we present the relativistic approach including spin-orbit interaction for the diatomic RbBa neutral molecule. The inclusion of spin-orbit coupling in the MRCI calculation was achieved when the total Hamiltonian $H = H_{el} + W_{so}$ is diagonalized on the basis of Λ-S states. H_{el} is the effective electrostatic Hamiltonian and W_{SO}^{PS} is the empirical spin-orbit pseudopotential which designed from the effective core potentials ECP to represent the spin-orbit effects in RbBa molecule defined as: $W_{SO} = \sum_A^{atom} U_{SO}(A)$, where for a given atom A, $U_{SO} = \sum_l U_l^{SO} P_l$. P_l is the projection operator into the subspace with angular symmetry l and $U_l^{SO}(r) = \sum_i C_{li} r^{n_{li}} e^{-\alpha_{li} r^2}$ is the spin orbit relativistic effective potential where the C_{li}, are the fitted parameters coefficients represented in section 2. The energies of the molecular states Ω including the spin-orbit effects have been obtained by diagonalizing the total Hamiltonian H_t in the basis of Λ states yielding the spin-orbit electronic states Ω = |Λ±∑| = 1/2, 3/2, 5/2, 7/2. All potential energy curves with spin-orbit coupling splitting have been calculated. Sixteen Λ-S states associated with the first five dissociation limits are splited into 33Ω states which consist of sixteen $\Omega_{1/2}$, eleven $\Omega_{3/2}$, five $\Omega_{5/2}$ and one $\Omega_{7/2}$ components. This relativistic treatment is necessary for an accurate description of the molecule because Rb and Ba are both heavy atoms with a significant spin-orbit splitting. The atomic spin-orbit splitting values are ($^2P^\circ_{3/2}$–$^2P^\circ_{1/2}$) =238 cm^{-1} for Rb, as well as for Ba($^3D_2$–$^3D_1$)=182 cm^{-1},

($^3D_3$–$^3D_2$)=381 cm^{-1}, ($^3P^\circ_1$–$^3P^\circ_0$)=317 cm^{-1} and($^3P_2$–$^3P_1$)=878 cm^{-1}. The potential energy curves of all Ω states are found to be bound states and are illustrated in **Figures 2(a, b et c)** respectively for Ω=1/2, Ω=3/2 and Ω=5/2,7/2 states resulting from the interaction of the orbital angular momentum Λ with the spin angular momentum S projected along the internuclear distance Σ. The spin-orbit coupling does not affect significantly the general profiles of the potential energy curves but new electronic states are generated. Also, abrupt variations of the higher excited potential energy curves are observed due to the presence of numerous avoided crossings between neighbor excited Ω states induced by the mixing of different states due to the spin-orbit interaction. In addition, the splitting of the Λ states may change rather the shape of the potential energy curves, and could thus modify the values of the spectroscopic parameters mainly the excitation energy T_e. So, the spectroscopic parameters for each low lying excited Ω states have been extracted and presented in **Table 4**. Also, the composition of low lying Ω-state wave functions, in terms of Λ-states (in percentage) at their equilibrium distance R_e are provided in **Table 5**. For each Ω state there is a predominant component Λ with a contribution larger than 88% so that the main parent Λ-S is identified. Nevertheless, there are states for which a small but significant contribution of other Λ states is obtained, which shows the mixing of different Λ states due to the spin-orbit interaction. Noting that the spectroscopic constants for Ω states just deviate slightly from those of their parent Λ-S states and the spin-orbit coupling effect change the R_e and D_e values, although not significantly. We note that the $^2\Sigma^+$states do not split with the Spin-orbit and only one state $\Omega_{1/2}$ is generated from each one. Indeed, the potential energy curves for $X^2\Sigma^+_{1/2}$, $(2)^2\Sigma^+_{1/2}$, $(3)^2\Sigma^+_{1/2}$, $(4)^2\Sigma^+_{1/2}$ states are nearly identical to their Λ-S states with a very close spectroscopic parameters. Noting that the $^2\Pi$ and $^2\Delta$ states are splitted into two Ω states ($^2\Pi_{1/2}$ and $^2\Pi_{3/2}$) and ($^2\Delta_{3/2}$ and $^2\Delta_{5/2}$) respectively. Also, $^4\Pi$ and $^4\Delta$, are splitted respectively into four Ω states (two $^4\Pi_{1/2}$, $^4\Pi_{3/2}$ and $^4\Pi_{5/2}$) and ($^4\Delta_{1/2}$, $^4\Delta_{3/2}$, $^4\Delta_{5/2}$, $^4\Delta_{7/2}$). The $^4\Sigma^+$ state is splitted into two Ω states ($^2\Sigma^+_{1/2}$ and $^2\Sigma^+_{3/2}$). We represent in **Figure 3** the parent electronic Λ states together with their respective daughter states Ω to illustrate the spin-orbit coupling effect on the dissociation energies T_e. As can be seen in this figure, the $(1)^2\Pi$ state is splitting into two states: $(1)^2\Pi_{1/2}$ and $(1)^2\Pi_{3/2}$ and the difference between the upper energy splitting and the lower one is 258 cm^{-1}. From **Table 5**, we note that their spectroscopic constants for the $(1)^2\Pi_{1/2}$ and $(1)^2\Pi_{3/2}$ are quite close with the same value of the equilibrium distances R_e. Compared to their $(1)^2\Pi$ parent state, we note a difference in the equilibrium distances by about ΔR_e =0.03 Bohr and a decrease in the depths of the wells by about 119 and 356 cm^{-1}compared to their $1^2\Pi$ parent. Also, the $(1)^2\Delta$ state is splitting into two states: $(1)^2\Delta_{3/2}$ and

$(1)^2\Delta_{5/2}$with dissociation energy difference by about 365 cm^{-1}. As represented in **Figure 3**, four states $(1)^4\Pi_{1/2}$, $(1)^4\Pi_{1/2}$, $(1)^4\Pi_{3/2}$ and $(1)^4\Pi_{5/2}$ have been splitting from their parent $(1)^4\Pi$ state with about 228 cm^{-1} difference between the upper and the lower energy splitting. The splitting effect on the $(1)^4\Delta$ electronic state is also represented in the same **Figure 3**. Unlike their parent $(1)^4\Delta$ which present with a single minima, the corresponding spin-orbit $(1)^4\Delta_{1/2}$, $(1)^4\Delta_{3/2}$ states present double minima and the large difference of the spectroscopic parameters is due to the high contribution and the mixing of numerous other states. In the side of the $(1)^4\Delta_{5/2}$ and $(1)^4\Delta_{7/2}$ spin-orbit states, each one present single minima with spectroscopic parameters very close to those obtained for $(1)^4\Delta$. For the higher excited Ω states, the shapes of the potential energy curves are more complicated and they interact much more with the presence of the avoided crossings between states of same symmetry. They present discontinuity and kink, originated from the contribution of $^{2,4}\Sigma^-$ states from higher asymptotes (see Figure 1), due to the mixing between their parent Λ-S states and the $1^4\Sigma^-$ state because of the spin-orbit coupling effect.

3.4 Permanent and Transition Dipole Moment

3.4.1 Permanent dipole moments of the ground state $X^2\Sigma^+$

For the RbBa molecule, only the permanent dipole moment of the ground state was determined by Gou et al **[22]**. To verify the reliability of our calculations, we have drawn in **Figure 4** the permanent dipole moment of the ground state $X^2\Sigma^+$ as a function of internuclear distances, calculated in the framework of this work (multiplied by two) with the theoretical results of reference **[22]**. A similar behavior is pointed out, the permanent dipole moment increases gradually to reach a maximum at almost the same internuclear distance R localized at 8.49 Bohr near the equilibrium distance. At the dissociation limit, the dipole moment of the ground state decreases and tends to zero. Our values of the dipole moments are lesser than those of Gou et al. because we used large-core pseudopotential while they used small-core pseudopotential for the polarization of the nucleus. It is noted that the implementation of the polarization of the nucleus using large-core pseudopotential leads to about 50% reduction of the absolute value of the dipole moment obtained by Gou et al **[22]**. The discrepancy can be explained also by the use of different basis sets, where we have used a larger one. In addition, we do not add the term of core polarization on the dipole. This term can affect the permanent dipole but not the transition one. In fact, the implementation of the polarization of the nucleus using large-core pseudopotential leads to about 50% reduction of the absolute value of the

dipole moment. The influence of the basis set size and the implementation of core polarization on the permanent dipole moments is discussed in the previous works **[28, 32, 33]**. Kotochigova et al **[32]** indicate also that the implementation of core polarization effects may reduce their dipole moment by about 50%. Unfortunately, there is no experimental value to compare with.

3.4.2 Permanent dipole moments of excited states

The permanent dipole moments were also calculated for the excited electronic states of the $^{2,4}\Sigma^+$, $^{2,4}\Pi$, and $^{2,4}\Delta$ symmetries. They are presented in **Figure 5** for the RbBa molecule. As it can be seen in **Figure 5**, the magnitudes of the permanent dipole moments are significant at short and medium internuclear distances. This behavior characterizes the Alk-Ba systems as polar molecules, which is crucial for the study of long-range dipole-dipole anisotropic interactions **[34]** controlled by an external electric or magnetic field allowing the control of the quantum dynamics of these molecules **[35]**. Also, the variation of the permanent dipole moment is marked by some remarkable abrupt changes, which are directly related to the avoided crossings presented in the potential energy curves. Nevertheless, a smooth variation is manifested at large internuclear distances where the permanent dipole moments of all the electronic states tend towards zero revealing the neutral character of these states in the vicinity of the dissociation limits.

3.4.3 Transition dipole moments

Indeed, the calculation of the Einstein coefficients, the radiative lifetimes and the photoassociation simulating process requires the determination of the transition dipole moments. Thus, the transition dipole moments are calculated between states in the same and different symmetries for the RbBa molecule. Noting that the transitions $\Sigma^+ \rightarrow \Delta$, are forbidden due to the selection rule. **Figure 6** presents the transition dipole moments from the ground state $X^2\Sigma^+$ to the excited states in $^2\Sigma^+$ and $^2\Pi$ symmetries.

At short internuclear distance, the transition dipole moments present peaks commonly related to the avoided crossings and to the charge transfer between the corresponding electronic states of the same symmetry. Indeed, the maximum value of the transition dipole moment is equal to 3.93 a.u corresponding to the transitions between the electronic states $X^2\Sigma^+$ and $(3)^2\Sigma^+$. It is due to the important overlap of the wave functions between these two states. In contrast to the case of permanent dipole moments, the asymptotic values of transition dipole moments are different for various transitions. For example, the transition

$X^2\Sigma^+ \rightarrow (4)^2\Sigma^+$ and $X^2\Sigma^+ \rightarrow (3)^2\Pi$ tend asymptotically to a constant equal to 3.2 a.u at large internuclear distances (R>20.0 Bohr) corresponding to the atomic allowed Rb(^{2}S) →Rb (^{2}P^o) transition which is close to the experimental value, 4.2 a.u **[27]**. As a result of the forbidden transition from Ba (^{1}S) to Ba (^{1,3}D and ^{3}P), the $X^2\Sigma^+ \rightarrow$ (2, 3, 5)$^2\Sigma^+$ and the $X^2\Sigma^+ \rightarrow$ (1, 2, 4) $^2\Pi$ transition dipole moments go to zero at large R.

3.4.4 Permanent and transition dipole moment including the Spin-Orbit coupling effects

The permanent and transition dipole moments of different spin-orbit component of Λ-S states are also determined. The PDM curves of the low lying Ω states (eight states for Ω=1/2, five states for Ω=3/2, three states for Ω=5/2 and one for Ω=7/2) represented in the **Supplementary Material (S. Fig 1)**. Note that the shape of the permanent dipole moment curves of components of each Λ-S remains almost the same and slightly shifted compared to the parent states. The **S. Fig 2** (**Supplementary Material)** exhibits the transition dipole moments of the low-lying excited spin-orbit state to the ground electronic state $^2\Sigma^+_{1/2}$. As it can be seen, the avoided crossings exist between the potential energy curves influence the transition dipole moments with several abrupt changes. Furthermore, for the higher excited states the behavior of the transition dipole moment became more and more complicated with some jumps, discontinuities and abrupt changes as the interaction between adjacent spin-orbit states of the same multiplicities and symmetries are significant especially at the position of the avoided crossings when the change of the electronic characteristics occurs to the mixing of Λ-S states due to spin orbit effects.

3.5 Vibrational Energy Levels, Radiative lifetimes and Franck–Condon factors: The feasibility of the laser-cooling of RbBa molecule:

Based on the obtained potential energy curves, the vibrational energy levels of the sixteen electronic states of the RbBa molecule are calculated by solving the radial Schrödinger equation using the Numrov algorithm. The spacing between the vibrational levels of all states in the $^{2,4}\Sigma^+$, $^{2,4}\Pi$ and $^{2,4}\Delta$ symmetries are presented in **Supplementary Material (S. Fig 3, S. Fig 4, S. Fig 5)**. Note that the vibrational energy spacing is far from being constant which is related to the anharmonicity of the potential wells. Initially, for the first vibrational levels, the spacing curves for numerous states of different symmetries are obtained with a linear variation corresponding to Morse-like anharmonic shape in potential energy curves. After that, the variation becomes smaller and vanishes at the dissociating limit. Note also that for the ground state and the low laying excited states, the vibrational levels are very numerous

and tight due to the significant well depths (several thousands of cm^{-1} as listed in table 3) and also to the anharmonicity of the potential wells, and they are found to be 82, 157, 156, 195 and 105 vibrational levels for $X^2\Sigma^+$, $(2)^1\Sigma^+$, $(3)^2\Sigma^+$, $(4)^2\Sigma^+$, and $(5)^2\Sigma^+$ states, respectively. For $(1)^2\Pi$, $(2)^2\Pi$, $(3)^2\Pi$ and $(4)^2\Pi$ states, the numbers of vibrational energy levels are respectively 169, 165, 137 and 87. It is clear that the states of symmetries $^2\Sigma^+$ and $^2\Pi$ have larger number of vibrational states compared to $^4\Sigma^+$ (85 and 79 vibrational level for $(1)^4\Sigma^+$ and $(2)^4\Sigma^+$ respectively) and (99 and 114 for $(1)^4\Pi$ and $(2)^4\Pi$ respectively) this result confirms our obtained spectroscopic parameters calculated previously, and indicates that the $^2\Sigma^+$ and $^2\Pi$ states have the deepest potential wells, which signifies that the RbBa molecule is more stable in these doublet states.

Moreover, the lifetime of the vibrational level is the main criteria that determine the feasibility of laser cooling. Firstly, the lifetime of the ground state $X^2\Sigma^+$ of RbBa molecule is calculated including the spontaneous emission and the Black Body Radiation (BBR), which is coming from the surrounding environment at T = 300 K and inducing stimulated absorption and emission processes as described in reference **[36]**.The vibrational energies and the corresponding lifetimes of the ground state $X^2\Sigma^+$ are listed in **Table 5**. Note that the lifetimes of the lowest vibrational states of RbBa are more than 10^4 s. The ground vibrational state $v=0$ has the longest life time with 124.171 10^3 s. After an initial decay, as a function of v, the lifetime reaches a minimum and then increases. The smallest value of the radiative lifetime is obtained for the vibrational state ν = 37, it is about 437.985 s. These values are useful for ultracold experiments, such as long-range dipole-dipole interactions and precise measurements for testing time variance of the proton-to-electron mass ratio **[35]** and are in reasonable agreement with similar systems **[36-37]**.

Thereafter, the vibrational radiative lifetimes of $A^2\Sigma^+$ and $A^2\Pi$ states are also calculated taking into account the two possible transitions: *bound-bound* and *bound-free*. The second contribution is calculated using the "*Franck-Condon*" approximation **[30, 38]**. The results are presented in **Figure 7**. The radiative lifetimes for the $A^2\Sigma^+$ ($v'=0$) and $A^2\Pi$ ($v''=0$) are 1.667 10^{-3} s and 0.546 10^{-3} s. The radiative lifetimes of the vibrational state for both $A^2\Sigma^+$ (v') and $A^2\Pi$ (v'') are initially rapidly decrease to reach a minimum respectively at v' =63 and $v''=86$, then increases to reach a larger values.

The possibility of laser cooling of Alkali-Alkaline earth species are largely discussed **[39-44]**. So, this part is devoted to study the possibility of cooling of RbBa molecule by direct laser cooling. In fact, the promising candidate molecules must meet up certain criteria: highly diagonal Franck–Condon factors (FCFs), short lifetime and no intervening electronic states.

From a practical standpoint, the highly diagonal Franck Condon Factors may limit the number of lasers required to keep the molecule in a closed-pumping cooling cycle and high spontaneous-emission rates, between two considered states, is necessary to describe rapid laser cooling. As the $A^2\Sigma^+$ and $A^2\Pi$ states are identified as the lowest excited states and no intermediate state could affect the laser cooling cycle between them and the ground state $X^2\Sigma^+$ via the spontaneous decay, the Franck-Condon overlaps of the $A^2\Sigma^+(v')\rightarrow X^2\Sigma^+(v)$ and $A^2\Pi(v'') \rightarrow X^2\Sigma^+(v)$ were evaluated from the corresponding vibrational eigen-functions. The Franck-Condon factors, expressed as three dimensional intensity plots, describe the overlap of the vibrational wave functions for $A^2\Sigma^+(v')\rightarrow X^2\Sigma^+(v)$ and $A^2\Pi\ (v'') \rightarrow X^2\Sigma^+(v)$ transitions are plotted in **Figures 8** and **9**. It is clear that for both transitions the values of the Franck-Condon factor is off diagonal with maximum of 0.5318 and 0.7405 obtained respectively for $A^2\Sigma^+(v'=154) \rightarrow X^2\Sigma^+(v=81)$ and $A^2\Pi\ (v''=161) \rightarrow X^2\Sigma^+(v=78)$ transitions. Most Franck-Condon factors of experimental cooling molecules should be greater than 0.9 as cited in many previous works **[39-44]**. In addition, small values of f_{00}=0.0001364 and f_{00}=4.054 10^{-11} for the both $A^2\Sigma^+\ (v'=0) \rightarrow X^2\Sigma^+(v=0)$ and $A^2\Pi(v''=0) \rightarrow X^2\Sigma^+\ (v=0)$ bands respectively, indicate that these two transitions pose quite minor probability, which is against the key ingredient of highly diagonal vibrational branching ratio. This unfeasibility can also be predicted from the fact that the values of equilibrium distances, R_e= 7.78 and 7.37 Bohr for $A^2\Sigma^+$ and $A^2\Pi$ states, are significantly different from that of $X^2\Sigma^+$ (R_e= 8.75 Bohr), and sufficient overlap of their vibrational wave functions cannot be achieved for the RbBa molecule. Despite, the excited state $3^2\Pi$ and the ground state $X^2\Sigma^+$ have comparable equilibrium distances at R_e=8.72 Bohr and R_e=8.75 Bohr, respectively. Thus, the radiative decay from $3^2\Pi \rightarrow X^2\Sigma^+$ will lead to the failure of a closed more than one-level transition cycle. We can conclude that, the main criteria for laser cooling of RbBa cannot be satisfied for transitions originating from the low-lying excited states to the ground state, which implies that the RbBa molecule is an inappropriate candidate for laser cooling.

4. CONCLUSION

In the present work, we have aimed extensive theoretical investigations for the low-lying electronic states that correlate with the first five dissociation asymptotes of RbBa molecule at the MRCI+Q level of calculation with large relativistic effective core potential ECP36 for Rb and ECP54 for Ba atoms and optimized basis set. The potential energy curves and the spectroscopic parameters for $16(^{2,4}\Sigma^+,^{2,4}\Pi,^{2,4}\Delta)$ first electronic states with respect to the lowest five dissociation limits were calculated. Excellent agreement for the spectroscopic constants

of the ground state with the only available reference demonstrates the reliability of our work. Spin-orbit calculation was also performed using relativistic pseudopotential approach and a shift of spectroscopic parameters between the Λ-S states and their related Ω states is detected and affected mainly T_e. Based on potential energy curves, permanent and transition dipole moments and vibrational wave functions, the vibrational lifetimes were evaluated for several states: $X^2\Sigma^+$, $A^2\Sigma^+$ and $A^2\Pi$. According to the Franck Condon factors calculation and the transition properties, direct laser cooling for RbBa is considered infeasible. Since no literature has reported for the spectroscopic parameters of the excited Λ-S states and all Ω states, to our knowledge, it is impossible for us to perform detailed comparisons with other studies. The resulting data can allow us to understand and analyze the structure, the bonding nature, the spectroscopic features, the chemical activities, and the reaction dynamics of RbBa molecule. Indeed, this work provides an opportunity to fill our knowledge gap and can be a helpful reference for the photo-association experiment of RbBa molecule.

Reference

[1] Quéméner G., Bohn J. , "*Shielding* $^2\Sigma^+$ *ultracold dipolar molecular collisions with electric fields*", **Phys. Rev. A 2016, 93, 012704.** DOI :10.1103/PhysRevA.93.012704.

[2] Carr L. D., DeMille D., Krems R.V., Ye J.," *Cold and ultracold molecules: science, technology and applications*", **New J. Phys. 2009, 11 055049**. DOI:10.1088/1367-2630/11/5/055049.

[3] Chen T., Zhu S., Li X., Qian J., Wang Y., "*Prospects for transferring* $^{87}Rb^{84}Sr$ *dimers to the rovibrational ground state based on calculated molecular structures*", **Phys. Rev. A 2014, 89, 063402**. DOI: 10.1103/PhysRevA.89.063402.

[4] Barbé V., Ciamei A., Pasquiou B., Reichsöllner L., Schreck F., Żuchowski P. S., Hutson J. M., "*Observation of Feshbach resonances between alkali and closed–shell atoms"* **Nature Physics 2018, 14.9, 881.** DOI: 10.1038/s41567-018-0169-x.

[5] Kajita M., Gopakumar G., Abe M., Hada M., "*Sensitivity of vibrational spectroscopy of optically trapped SrLi and CaLi molecules to variations in* m_p/m_e"**, J. Phys. B: Atomic, Molecular and Optical Physics, 2012, 46.2, 025001.** DOI:10.1088/0953-4075/46/2/025001/meta.

[6] Ciamei A., Szczepkowski J., Bayerle A., Barbé V., Reichsöllner L., Tzanova S. M., Jastrzebski W., **"***The RbSr* $^2\Sigma^+$ *ground state investigated via spectroscopy of hot and ultracold molecules***". Phys. Chem. Chem. Phys, 2018, 20, 26221-26240.** DOI: 10.1039/C8CP03919D.

[7] Lackner F., Krois G., Buchsteiner T., Pototschnig J.V., Ernst W.E., "*Helium-droplet-assisted preparation of cold RbSr molecules*", **Phys. Rev. Lett. 2014,113, 153001.** DOI: 10.1103/PhysRevLett.113.153001.

[8] Micheli A., Brennen G. K., Zoller P., "*A toolbox for lattice-spin models with polar molecules*", **Nat. Phys., 2006,2, 341-347.**DOI: https://doi.org/10.1038/nphys287.

[9] Pérez-Ríos J., Herrera F., Krems R. V., "*External field control of collective spin excitations in an optical lattice of* $^2\Sigma^+$ *molecules"*, **New J. Phys. 2010, 12, 103007.** DOI: 10.1088/1367-2630/12/10/103007/meta.

[10] Gopakumar G., Abe M., Kajita M., Hada M., " *Ab initio study of permanent electric dipole moment and radiative lifetimes of alkaline-earth-metal--Li molecules*", **Physical Review A 2011, 84.6, 062514.** DOI: https://doi.org/10.1103/PhysRevA.84.062514.

[11] Pototschnig J. V., Krois G., Lackner F., Ernst W. E.," *Investigation of the RbCa molecule: Experiment and theory*" , **J. Mol. Spectrosc, 2015, 310, 126**. DOI: https://doi.org/10.1016/j.jms.2015.01.006.

[12] Pototschnig J. V., Krois G., Lackner F., Ernst W. E., *"Characterization of RbSr molecules: spectral analysis on helium droplets*", **J. Chem. Phys., 2014, 141, 234309.** DOI: https://doi.org/10.1039/C4CP03135K.

[13] Lackner F., Krois G., Buchsteiner T., Pototschnig J. V., Ernst W. E.," *Helium-droplet-assisted preparation of cold RbSr molecules*", **Phys. Rev. Lett., 2014, 113, 153001.** DOI: https://doi.org/10.1103/PhysRevLett.113.153001.

[14] Adrien D., Eliane L. K., Osman A., Michèle D. L., Olivier D., **"***Laser-Assisted Self-Induced Feshbach resonance for ultracold polar molecule formation"***, Phys. Rev. A; 2019, 1902, 00323.** DOI: 10.1103/PhysRevA.100.052703.

[15] You Y., Yang C. L., Wang M. S., Ma X. G., Liu W. W., Wang L. Z., "*Construction of analytic functions for the potential energy curves, dipole moments, and transition dipole moments of RbBe and CsBe molecules*". **J. Quant. Spect. Radia.Trans., 2015, 165, 56-67.** DOI: https://doi.org/10.1016/j.jqsrt.2015.06.026

[16] Houalla D., Chmaisani W., El-Kork N., Korek M., "*Electronic structure calculation of the MgAlk (Alk= K, Rb, Cs) molecules for laser cooling experiments*". **Compt. Theor. Chem, 2017, 1108, 103-110.** DOI: https://doi.org/10.1016/j.comptc.2017.03.009.

[17] Gopakumar G., Abe M., Hada M., Kajita M., "*Dipole polarizability of alkali-metal (Na, K, Rb)–alkaline-earth-metal (Ca, Sr) polar molecules: Prospects for alignment*". **J. Chem. Phys., 2014, 140, 224303.** DOI: https://doi.org/10.1063/1.4881396.

[18] Pototschnig J.V., Krois G., Lackner F., Ernst W. E., "*Ab initio study of the RbSr electronic structure: Potential energy curves, transition dipole moments, and permanent electric dipole moments*", **J. Chem. Phys. 2014, 141, 234309.** DOI : https://doi.org/10.1063/1.4903791.

[19] Devolder A., Luc-Koenig E., Atabek O., Desouter-Lecomte M., Dulieu O., "*Proposal for the formation of ultracold deeply bound RbSr dipolar molecules by all-optical methods*". **Phy. Rev. A, 2018, 98l, 053411.** DOI: https://doi.org/10.1103/PhysRevA.98.053411.

[20] Huang Y., Qi J., Pechkis H.K., Wang D., Eyler E.E., Gould P.L., Stwalley W.C., "*Formation, detection and spectroscopy of ultracold Rb_2 in the ground $X^1\Sigma_g^+$ state*", **J. Phys. B 2006, 39, 857–869.** DOI : 10.1088/0953-4075/39/19/S04.

[21] Anderson M. H., Ensher J.R., Matthews M.R., Wieman C.E., Cornell E.A., " *Observation of Bose-Einstein condensation in a dilute atomic vapor*", **Science 1995, 269, 198–201.** DOI: https://www.jstor.org/stable/2888436.

[22] Gou D., Kuang X., Gao Y., Huo D.," *Theoretical study on the ground state of the polar alkali metal-barium molecules: Potential energy curve and permanent dipole moment*", **J. Chem. Phy, 2015, 142, 034308.** DOI: https://doi.org/10.1063/1.4906049.

[23] Werner H. J., Knowles P. J., Knizia G., Manby F. R., Schütz M., *et al.*, .**MOLPRO version 2010**.1, a package of ab initio programs, 2010. see http://www.molpro.net.

[24] Stevens W. J., Krauss H., Basch H., Jasien P. G., "*Relativistic compact effective potentials and efficient, shared-exponent basis sets for the third-, fourth-, and fifth-row atoms*" **Can. J. Chem. 1992, 70, 612-630.** DOI: https://doi.org/10.1139/v92-085.

[25] Muller W., Flesch J., Meyer W., "*Treatment of intershell correlation effects in ab initio calculations by use of core polarization potentials. Method and application to alkali and alkaline earth atoms*." **J. Chem. Phys. 1984, 80, 3297.** DOI: https://doi.org/10.1063/1.447083

[26] Jones R. R., Gallagher T. F., "*Observation of $Ba^{+}np_{1/2}$ and ngj Rydberg series"*, **J. Opt. Sot. Am. B. 1989. 6, 1467-1472.** DOI: https://doi.org/10.1364/JOSAB.6.001467.

[27] Kramida A. E., Ralchenko Y., Reader J., NIST ASD Team, **NIST Atomic Spectra Database** (ver. 5.5.6), National Institute of Standards and Technology, Gaithersburg, MD **(2018).** DOI: https://dx.doi.org/10.18434/T4W30F.

[28] Ladjimi H. , Farjallah M., Mlika R., Allouche A. R., Berriche H.," *Ab initio calculations of electronic structure of the BaCs molecule: adiabatic potential energy curves, spectroscopic constants, spin–orbit effect and permanent and transition electric dipole moments*", **Theo. Chem. Accounts, 2019, 138, 56.** DOI: 10.1007/s00214-019-2443-0.

[29] Johnson B. R., "*The renormalized Numerov method applied to calculating bound states of the coupled-channel Schroedinger equation*". **J. Chem. Phys, 1978, 69(10), 4678-4688.** DOI: https://doi.org/10.1063/1.436421.

[30] Zemke W. T., Crooks J. B., StwalleyW. C., "*Radiative and nonradiative lifetimes for vibrational levels of the $A^{1}\Sigma^{+}$ state of ^{7}LiH*". **J. Chem. Phys. 1978, 68, 4628-4630.** DOI: https://doi.org/10.1063/1.435569.

[31] Jendoubi I., Berriche H., Ben Ouada H., Gadea F. X., "*Structural and spectroscopic study of the LiRb molecule beyond the Born–Oppenheimer approximation*". **J. Phys. Chem. A, 2012, 116, 2945-2960.** DOI: https://doi.org/10.1021/jp209106w.

[32] Kotochigova, S., Julienne, P. S., Tiesinga, E. "*Ab initio calculation of the KRb dipole moments*". ***Physical Review A*, 2003, *68*(2), 022501.** DOI: https: //doi.org/ 10.1103/ Phys Rev A.68. 022501.

[33] Aymar, M., Dulieu, O. "Calculation of accurate permanent dipole moments of the lowest $^{1,\ 3}\Sigma^{+}$ states of heteronuclear alkali dimers using extended basis sets". ***The Journal of chemical physics*, 2005, *122*(20), 204302**. DOI: https://doi.org/10.1063/1.1903944

[34] Idziaszek Z., Calarco T., Zoller P.,"*Controlled collisions of a single atom and an ion guided by movable trapping potentials*", **Phys. Rev. A. 2007, 76, 033409.** DOI: https://doi.org/10.1103/PhysRevA.76.033409.

[35] Ospelkaus S., Ni K. K., Wang D., de Miranda M. H. G., Neyenhuis B., Quemener G., Julienne P. S., Bohn J. L., Jin D. S., Ye J., "*Quantum-state controlled chemical reactions of ultracold potassium-rubidium molecules*"; **Science 2010, 327, 853.** DOI: 10.1126/science.1184121.

[36] Fedorov D. A., Derevianko A., Varganov S. A., "*Accurate potential energy, dipole moment curves, and lifetimes of vibrational states of heteronuclear alkali dimmers*". **J. Chem. Phys, 2014, 140(18), 184315.** DOI: https://doi.org/10.1063/1.4875038.

[37] Gopakumar G., ABE M., Kajita M., Hada M., "*Ab initio study of permanent electric dipole moment and radiative lifetimes of alkaline-earth-metal--Li molecules*". **Phys. Rev. A, 2011, 84, 6, 062514.** DOI: https://doi.org/10.1103/PhysRevA.84.062514.

[38] Mabrouk N. , Berriche H., "*Theoretical evaluation of the radiative lifetimes of LiCs and NaCs in the $A^1\Sigma^+$ state*", **Russ. J. Phys. Chem. A, 2017, 91 ,1474-1485.** DOI: 10.1134/S0036024417080192

[39] Zeid I., Atallah T., Kontar S., Chmaisani W., El-Kork N., Korek M.; "*Theoretical electronic structure of the molecules SrX (X= Li, Na, K) toward laser cooling study*". **Computational and Theoretical Chemistry, 2018, 1126, 16-32.** DOI: https://doi.org/10.1016/j.comptc.2018.01.013.

[40] Kang S., Gao Y., Kuang F., Gao T., Du J., Jiang G., "*Theoretical study of laser cooling of magnesium monofluoride using ab initio methods*". **Phys. Rev. A, 2015, 91(4), 042511.** DOI: https://doi.org/10.1103/PhysRevA.91.042511.

[41] You Y., Yang C. L., Wang M. S., Ma X. G., Liu W. W., "*Theoretical investigation of the laser cooling of a LiBe molecule*". **Phys. Rev. A, 2015, 92(3), 032502.** DOI: https://doi.org/10.1103/PhysRevA.92.032502

[42] Xu L., Yin Y., Wei B., Xia Y., Yin J., "*Calculation of vibrational branching ratios and hyperfine structure of ^{24}Mg ^{19}F and its suitability for laser cooling and magneto-optical trapping*". **Phys. Rev. A, 2016, 93(1), 013408**. DOI: https://doi.org/10.1103/PhysRevA.93.013408

[43] Yang R., Tang B., Han X., "*Laser cooling of InF, InCl and InH with an ab initio study*". ***RSC Advances*, 2019, *9*(54), 31543-31550**. DOI : 10.1039/C9RA03482J.

[44] Li C., Li Y., Ji Z., Qiu X., Lai Y., Wei J., Liu J.,"*Candidates for direct laser cooling of diatomic molecules with the simplest $^1\Sigma - ^1\Sigma$ electronic system*". **Phys. Rev. A, 2018, 97(6), 062501.** DOI: https://doi.org/10.1103/PhysRevA.97.062501.

TABLE 1. Calculated atomic energies level compared to the experimental results [27].ΔE gives the difference between the theoretical and the experimental energy. All values are given in cm^{-1}.

ion/atom	states	Exp[27]	This work	|ΔE1|
Rb	$4p^6 5s(^2S_{1/2})$	0	0	0
	$4p6 5p(^2P)$	12737	12737	0
	$4p6 5p(^2P_{1/2})$	12578	12578	0
	$4p6 5p(^2P_{3/2})$	12816	12816	0
	$4p^6 4d(^2D)$	19356	19355	1
	$4p^6 6s(^2S_{1/2})$	20130	20132	2
Ba^+	$6s^1(^2s)$	0	0	0
	$5d^1(^2D)$	5354	5356	2
	$5d^1(^2D_{3/2})$	4874	4933	59
	$5d1(^2D_{5/2})$	5675	5639	36
	$6p^1(^2P)$	21388	21382	6
	$6p^1(^2P_{1/2})$	20262	20256	6
	$6p^1(^2P_{3/2})$	21952	22059	107
Ba	$6s^2(^1S)$	0	0	0
	$6s^1 5d^1(^3D)$	9282	9251	31
	$6s^1 5d^1(^3D_1)$	9034	8934	100
	$6s^1 5d^1(^3D_2)$	9216	9117	99
	$6s^1 5d^1(^3D_3)$	9597	9463	134
	$6s^1 5d^1(^1D)$	11395	11455	60
	$6s^1 6p^1(^3P)$	13089	13177	88
	$6s^1 6p^1(^3P_0)$	12266	12331	65
	$6s^1 6p^1(^3P_1)$	12637	12700	63
	$6s^1 6p^1(^3P_2)$	13515	13600	85

TABLE 2. Asymptotic energies and electronic states of RbBa molecule. ΔE gives the difference between the calculated and the experimental energy. All the values are given in cm^{-1}.

Symmetry	dissociation limits	This work	Experiment[27]	ΔE
$^2\sum^+$	$Ba(6s^2(^1S))+Rb(4p^65s(^2S))$	0	0	0
$^{2,4}\sum^+,^{2,4}\Pi,^{2,4}\Delta$	$Ba(6s5d(^3D))+Rb(4p^65s(^2S))$	9251	9282	31
$^2\sum^+,^2\Pi,^2\Delta$	$Ba(6s5d(^1D))+Rb(4p^65s(^2S))$	11455	11395	60
$^2\sum^+,^2\Pi$	$Ba(6s^2(^1S))+Rb(4p^65p(^2P°))$	12737	12737	0
$^{2,4}\sum^+,^{2,4}\Pi$	$Ba(6s6p(^3P°))+Rb(4p^65s(^2S))$	13177	13098	79

TABLE 3. Spectroscopic Constants for the ground and low-lying excited Electronic Λ-S States of the RbBa Molecule

States	R_e (Bohr)	D_e (cm^{-1})	T_e (cm^{-1})	ω_e (cm^{-1})	$\omega_e\chi_e$(cm^{-1})	B_e (cm^{-1})	Ref
$X^2\sum^+$	8.75	1566	0	42.59	0.29	0.014934	**This work**
	9.31	1471	0	39.23	0.27	0.013300	[22]
$2^2\sum^+$	7.78	5661	5156	65.76	0.19	0.018903	**This work**
$3^2\sum^+$	8.80	4908	8114	54.53	0.15	0.014745	**This work**
$4^2\sum^+$	9.00	4986	9315	46.15	0.21	0.014114	**This work**
$5^2\sum^+$	11.15	1258	13482	15.69	0.05	0.009187	**This work**
$1^4\sum^+$	9.10	1203	9615	32.37	0.31	0.013795	**This work**
$2^4\sum^+$	11.03	712	14028	19.81	0.20	0.009394	**This work**
$1^2\Pi$	7.37	7825	2992	74.88	0.19	0.021014	**This work**
$2^2\Pi$	8.08	6273	6748	63.78	0.22	0.017491	**This work**
$3^2\Pi$	8.72	2786	11516	31.89	0.29	0.015024	**This work**
$4^2\Pi$	9.79	1018	13724	21.58	0.39	0.011921	**This work**
$1^4\Pi$	8.04	2357	8460	53.01	0.29	0.017824	**This work**
$2^4\Pi$	9.18	2326	12416	41.88	0.09	0.013569	**This work**
$1^2\Delta$	7.89	5086	5731	62.53	0.19	0.018351	**This work**
$2^2\Delta$	9.96	897	12127	24.43	0.20	0.011520	**This work**
$1^4\Delta$	10.48	439	10379	18.13	0.31	0.010414	**This work**

TABLE 4. The positions of Avoided Crossing between Neighbor Electronic States R_{AC} and the energy difference ΔE_{AC} at these positions.

State1/State2	R_{AC} (Bohr)	ΔE_{AC} (cm^{-1})
$2^2\sum^+/3^2\sum^+$	10.75	1360.19
$3^2\sum^+/4^2\sum^+$	6.6	1334.62
	11.15	535.51
	15.15	844.1
$1^2\Pi/2^2\Pi$	10.95	1367.54
$2^2\Pi/3^2\Pi$	13.15	998.61

TABLE 5. Spectroscopic parameters of the Ω states and therecomposition of Ω-state wave functions, in terms of Λ-states (in percentage) at the equilibrium distance R_e

Ω[Λ]	**R_e(Bohr)**	**D_e(cm^{-1})**	**T_e(cm^{-1})**	**ω_e (cm^{-1})**	**$\omega_e\chi_e$(cm^{-1})**	**B_e(cm^{-1})**	**% (Λ-parent)**
(1)1/2[$X^2\sum^+$]	8.75	1571	0	42.66	0.43	0.014956	99.89%[$X^2\sum^+$]
(2)1/2[$1^2\Pi$]	7.39	7634	2870	77.40	0.36	0.020952	98.52%[$1^2\Pi$]+1.27%[$X^2\sum^+$]
(1)3/2[$1^2\Pi$]	7.39	7469	3128	74.63	0.19	0.020955	99.38%[$1^2\Pi$]+0.44%[$X^2\sum^+$]
(3)1/2[$2^2\sum^+$]	7.78	5465	5131	65.71	0.20	0.018880	97.43 [$2^2\sum^+$]+1.17[$2^2\Pi$]
(2)3/2[$1^2\Delta$]	7.90	5057	5554	62.57	0.18	0.018334	98.88% [$1^2\Delta$]+0.52%[$1^2\Pi$]+0.6%[$2^2\Pi$]
(1)5/2[$1^2\Delta$]	7.89	4868	5919	62.65	0.19	0.018370	98.88%[$1^2\Delta$]+0.52%[$1^2\Pi$]+0.6%[$2^2\Pi$]
(4)1/2[$2^2\Pi$]	8.09	4068	6543	63.27	0 .15	0.017466	95.56%[$2^2\Pi$]+0.52%[$2^2\sum^+$]+1.34%3[$^2\sum^+$]
(3)3/2[$2^2\Pi$]	8.08	3802	6985	63.70	0.22	0.017486	99.11%[$2^2\Pi$]+0.32%[$1^2\Delta$]
(5)1/2[$3^2\sum^+$]	8.16 ^{min1}	2485	8302	28.52	0.08	0.017166	94.45% [$2^2\sum^+$]+3.76%[$2^2\Pi$]
	8.76 ^{min2}	2633	8154	55.37	0.30	0.014895	
(6)1/2[$1^4\Pi$]	8.06	2585	8372	54 .05	3.07	0.016986	94.44%[$1^4\Pi$]+0.37%[$1^4\sum^+$]+3.92% [$3^2\sum^+$]
(7)1/2[$1^4\Pi$]	6.89 ^{min1}	570*					95.55%[$1^4\Pi$]+0.73%[$1^4\sum^+$]+2.71% [$3^2\sum^+$]
	8.26 ^{min2}	2597	8437	109.98	11.68	0.016745	
(4)3/2[$1^4\Pi$]	8 .04	2463	8494	52.47	0 .40	0.017660	99.08%[$1^4\Pi$]+0.59%[$1^4\sum^+$]
(2)5/2[$1^4\Pi$]	8 .05	2357	8600	52.66	0 .59	0.017634	94.44%[$1^4\Pi$]+0.37%[$1^4\sum^+$]+3.92% [$3^2\sum^+$]
(8)1/2[$4^2\Sigma^+$]	9.00	3704	9330	46.17	0 .20	0 .014120	97.55%[$4^2\Sigma^+$]+2.12%[$1^4\Pi$]
(10)1/2[$1^4\Delta$]	7.54^{min1}	2988	11049	209.95			88.91%[$1^4\Delta$]+4.15%[$1^4\Pi$]+2.34%[$1^4\sum^+$]
	10.28^{min2}	3837	10200	23.25			
(6)3/2[$1^4\Delta$]	7.44 ^{min1}	2087	10942	211.79			92.56%[$1^4\Delta$]+6.84%[$1^4\Pi$]
	10.29 ^{min2}	2687	10342	21.67			
(3)5/2[$1^4\Delta$]	10.36	559	10470	20.01	0.24	0.010647	92.56%[$1^4\Delta$]+3.78%[$1^4\Pi$]
(1)7/2[$1^4\Delta$]	10.46	441	10588	18.2	0.31	0.010436	99.99%[$1^4\Delta$]

TABLE 6. Energies and Lifetimes of the vibrational states *v* of the electronic ground state $X^2\sum^+$ at T=300K for RbBa molecule.

v	Energy(cm^{-1})	Lifetimes(s)	*v*	Energy(cm^{-1})	Lifetimes(s)
0	0	124171.1945	42	947.9127	449.3656
1	31.824	36926.9942	43	961.7396	454.7153
2	63.4284	17928.9755	44	973.8107	461.1377
3	94.5939	10686.7589	45	985.6624	468.6764
4	125.1009	7149.4556	46	997.0751	477.3866
5	155.3884	5153.3157	47	1008.0488	487.3501
6	185.237	3914.9941	48	1018.5836	498.6966
7	214.6467	3093.0541	49	1028.8989	511.5696
8	243.3979	2519.0630	50	1038.7753	526.2449
9	271.9297	2102.0843	51	1048.4322	543.1041
10	300.0224	1789.5218	52	1057.4307	562.6337
11	327.6763	1549.1835	53	1066.2097	585.5853
12	354.6717	1360.4307	54	1074.5497	612.7673
13	381.4477	1209.5162	55	1082.4508	645.1543
14	407.7847	1087.0177	56	1089.913	683.4188
15	433.6827	986.3114	57	1097.1557	727.8893
16	459.1418	902.6126	58	1103.9594	778.2357
17	484.162	832.3934	59	1110.5436	833.3346
18	508.5237	773.0066	60	1116.6889	891.7671
19	532.666	722.4429	61	1122.3953	952.6603
20	556.3693	679.1531	62	1127.8821	1017.1874
21	579.4141	641.9171	63	1133.1496	1088.9370
22	602.2395	609.7763	64	1137.978	1174.6819
23	624.4065	581.9606	65	1142.587	1283.3211
24	646.1345	557.8503	66	1146.9765	1425.8431
25	667.2041	536.9416	67	1151.1465	1614.4848
26	688.0542	518.8261	68	1155.0971	1862.2778
27	708.2459	503.1615	69	1158.8281	2182.9209
28	727.7792	489.6628	70	1162.3397	2589.1276
29	746.8736	478.1058	71	1165.4124	3090.9698
30	765.5289	468.2923	72	1168.485	3698.9056
31	783.5259	460.0605	73	1171.3382	4425.9694
32	801.0839	453.2872	74	1173.7524	5300.3056
33	818.2029	447.8533	75	1176.1667	6366.8011
34	834.4441	443.6717	76	1178.1419	7715.6115
35	850.4658	440.6688	77	1180.1172	9488.8090
36	865.8291	438.7881	78	1181.4341	11901.9381
37	880.9728	437.9854	79	1182.7509	15229.3547
38	895.4581	438.2252	80	1183.6288	19820.1871
39	909.5045	439.4872	81	1184.5067	26376.3205
40	923.1121	441.7635	82	1185.1651	32277.8479

41	936.5001	445.0559

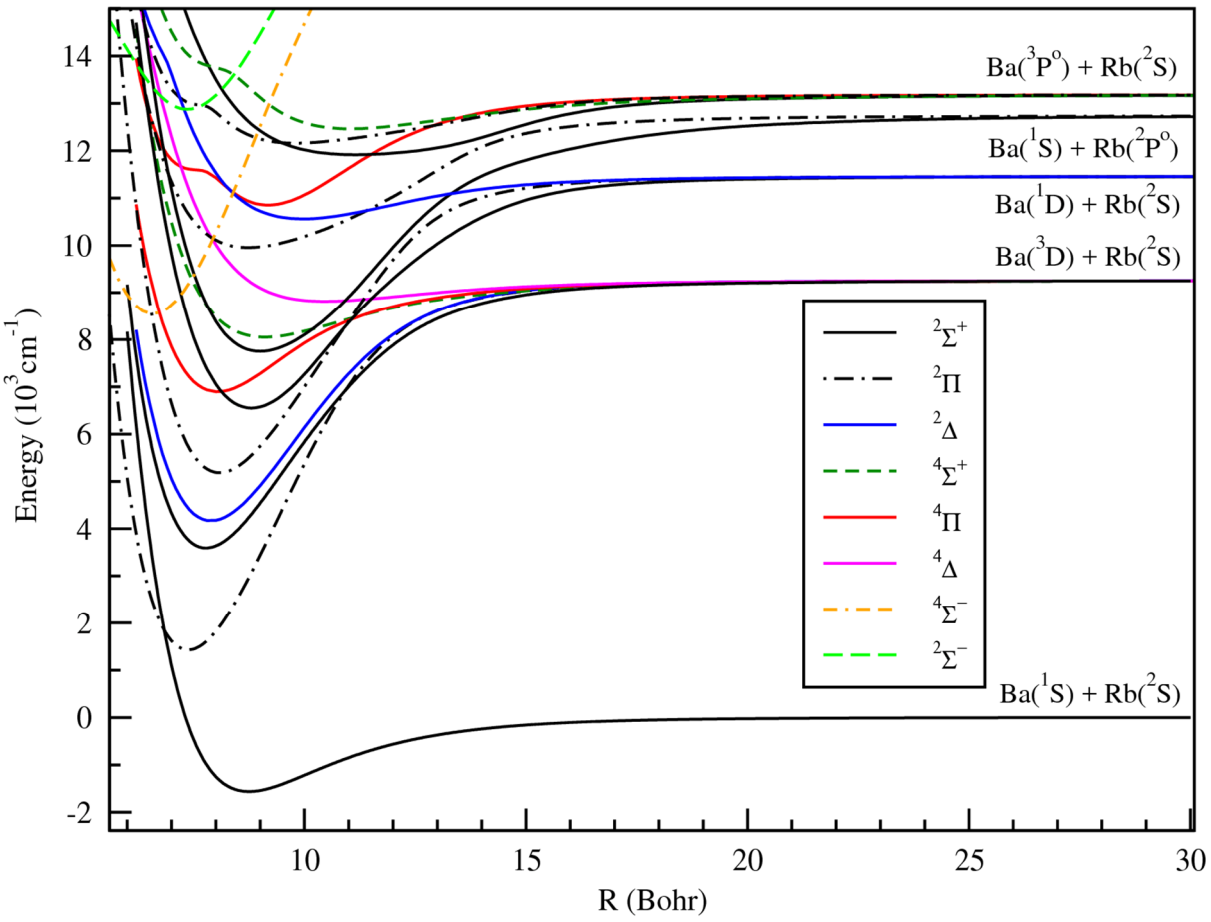

Figure 1: Potential energy curves for $^{2,4}\Sigma^+$, $^{2,4}\Pi$ and $^{2,4}\Delta$ symmetries states of RbBa dissociating into the first five asymptotic limit

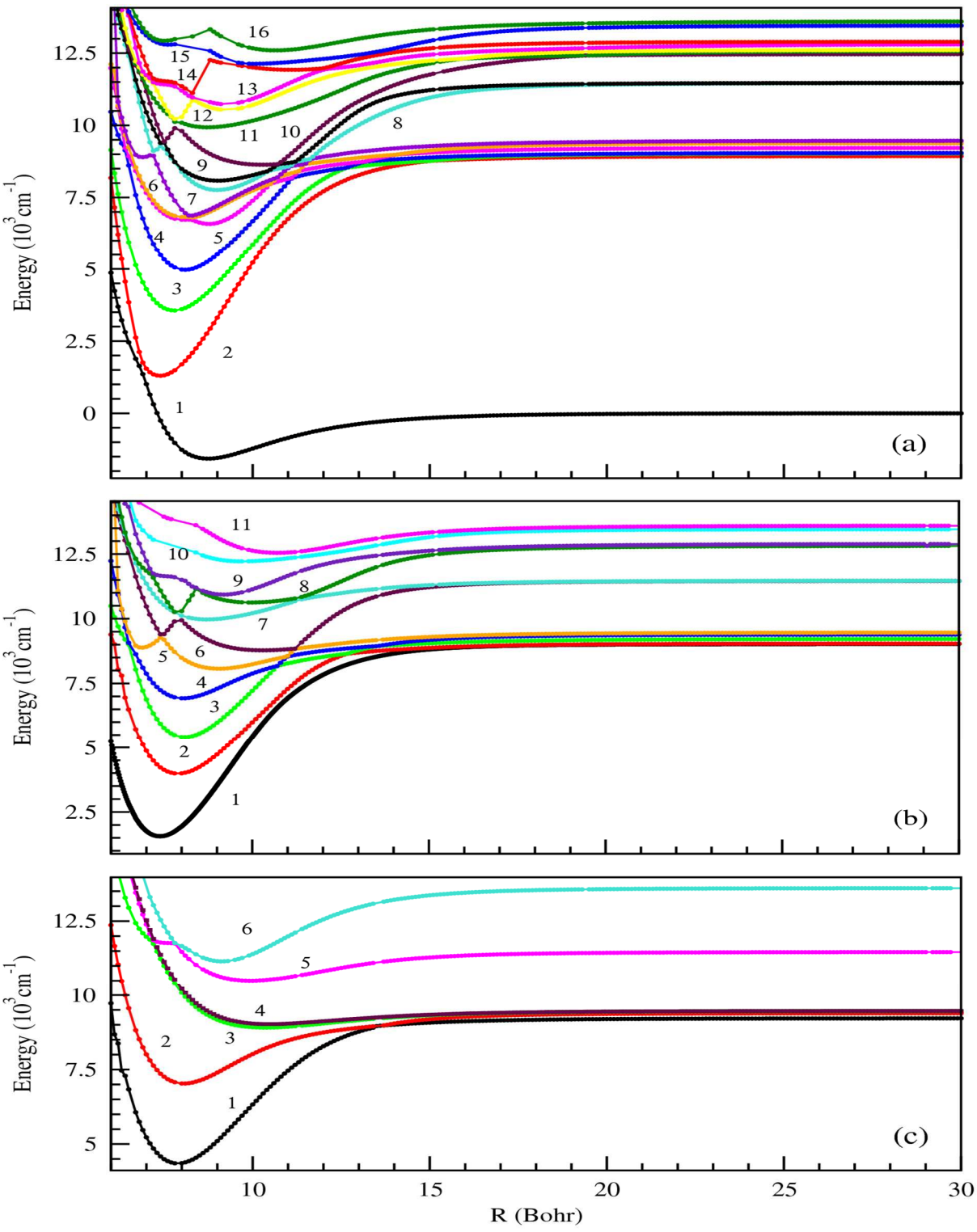

Figure 2: Potential energy curves of spin-orbit Ω states with Ω =1/2 **(a),** Ω =3/2 **(b)** and Ω=5/2, 7/2 **(c)**

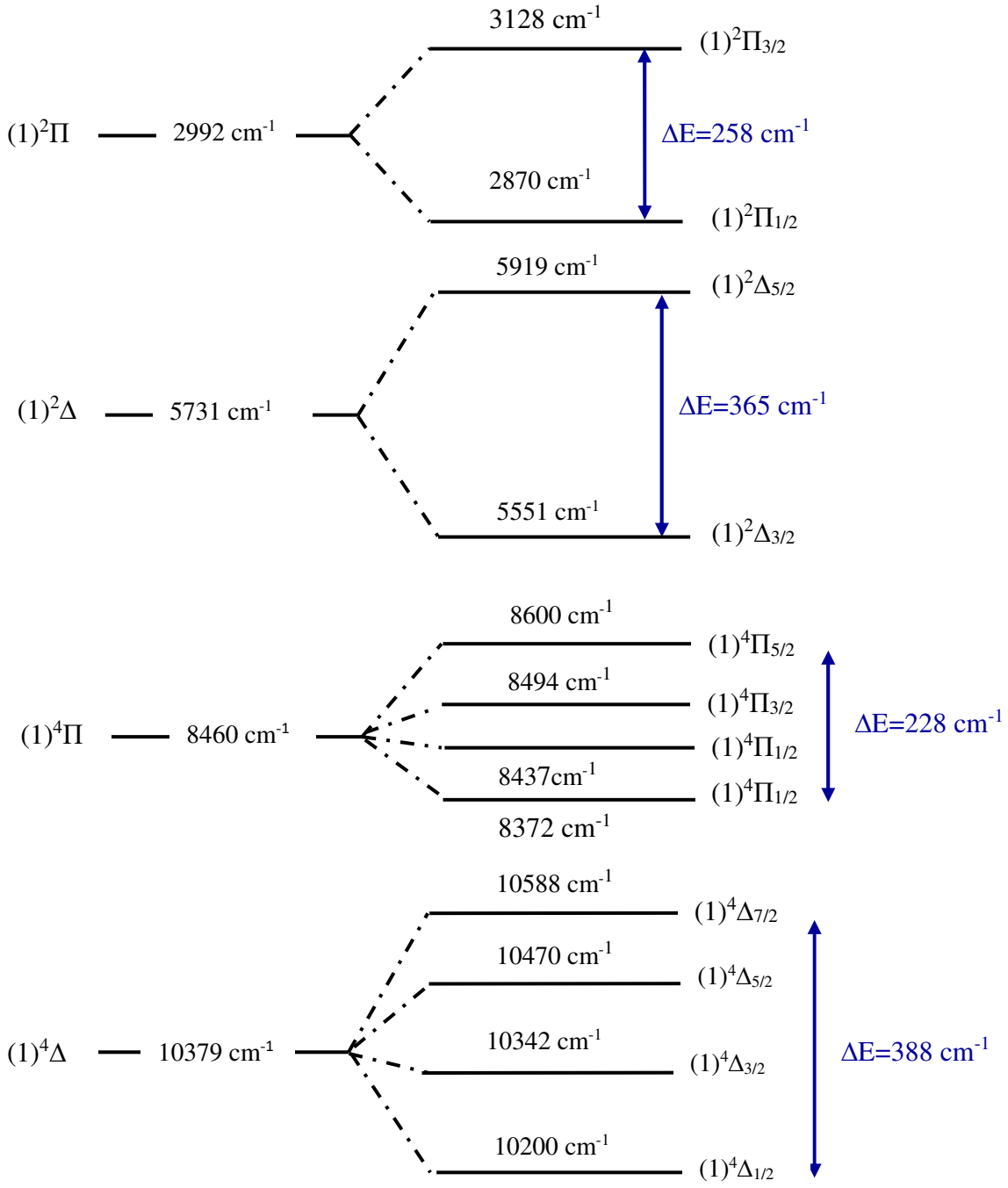

Figure 3: Spin-Orbit splitting occurring at equilibrium distances in the electronic states $1^{2,4}\Pi$ and $1^{2,4}\Delta$ of the RbBa molecule in cm^{-1}.

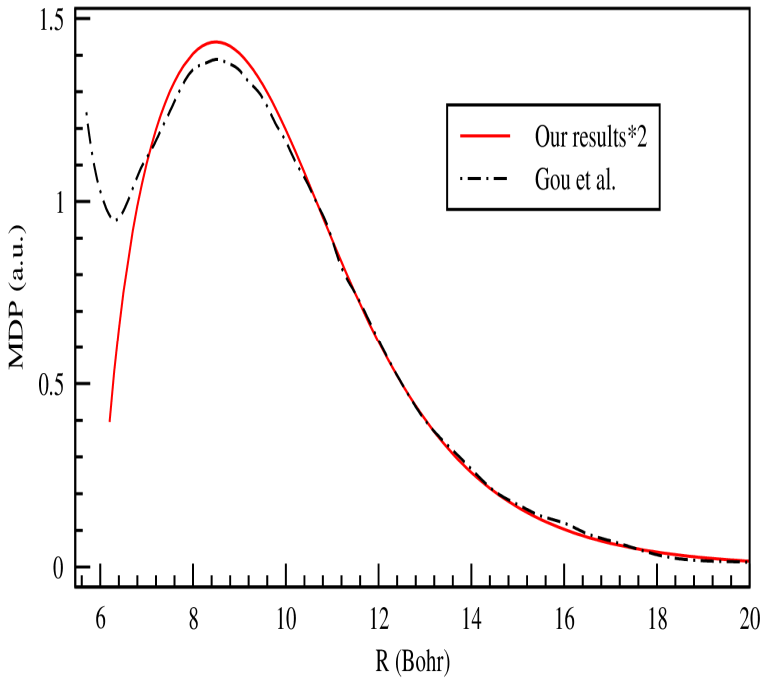

Figure 4: Permanent dipole moments for the ground $X^2\Sigma^+$ state multiplied by two RbBa molecule compared by that obtained by Gou et al **[22].**

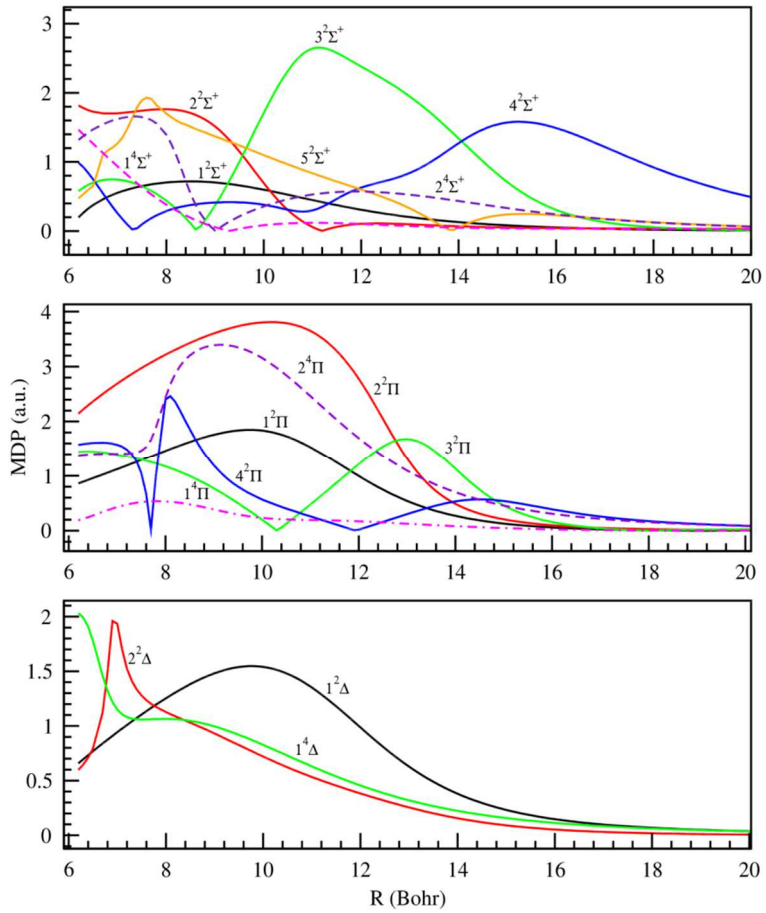

Figure 5: Permanent dipole moments for the $^{2,4}\Sigma^+$, $^{2,4}\Pi$ and $^{2,4}\Delta$ states of RbBa molecule

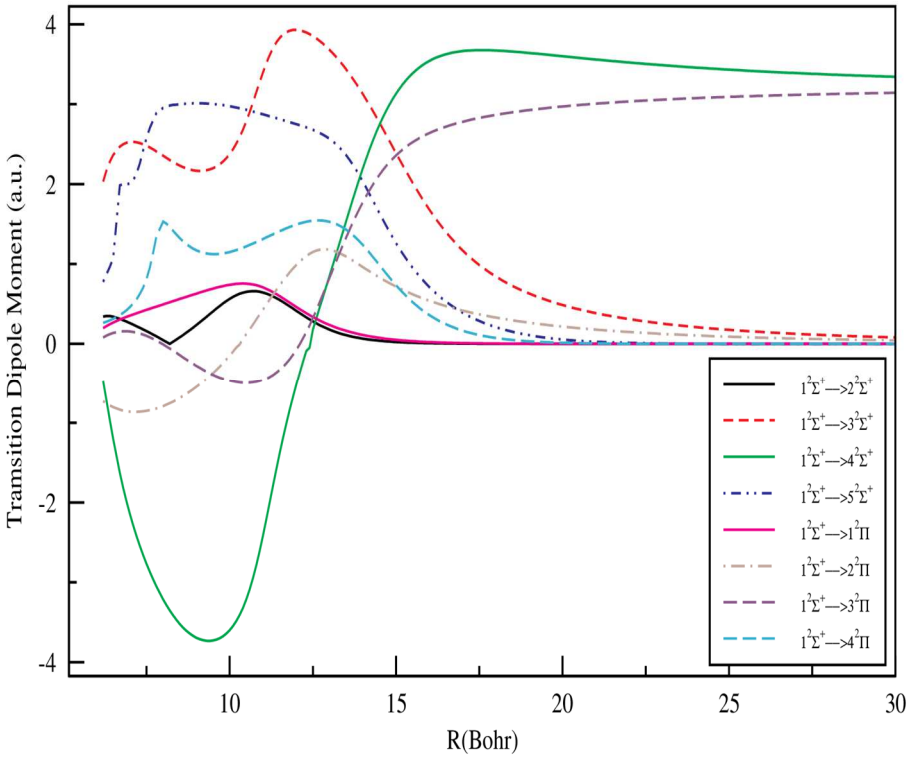

Figure 6: Transition dipole moments from some low-lying excited states to the ground state

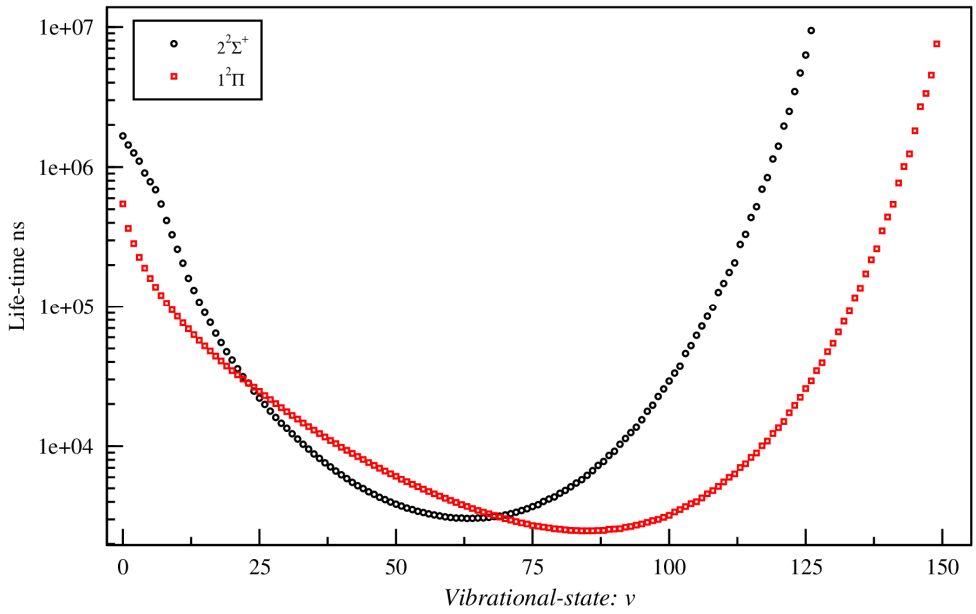

Figure 7: Vibrational Lifetimes of the $2^2\Sigma^+$, $1^2\Pi$ electronic states

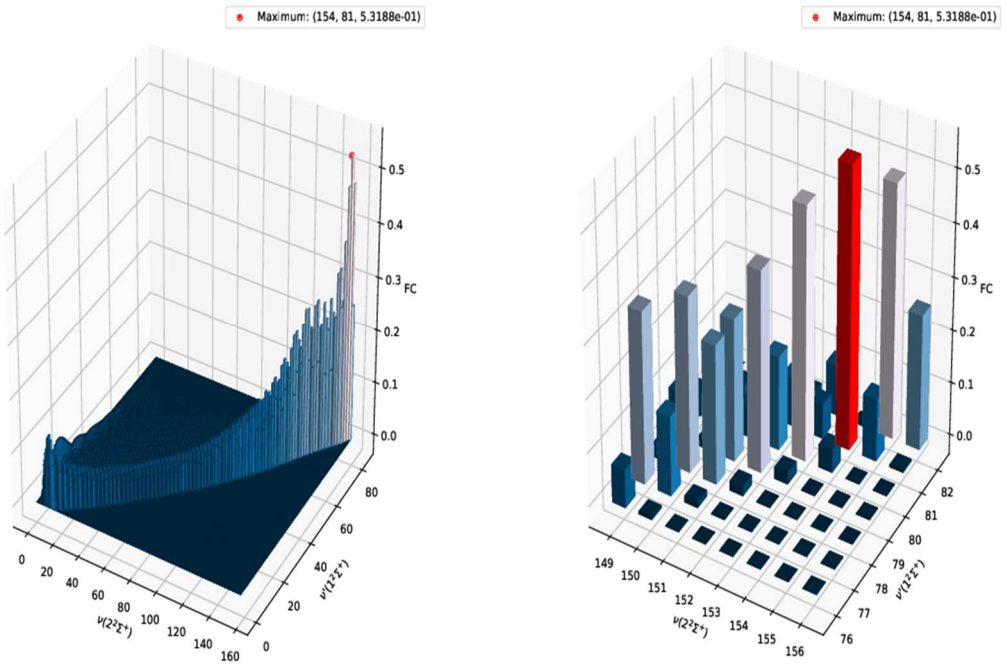

Figure 8: The calculated FCFs of RbBa for vibrational level of cooling transition $A^2\Sigma^+ \rightarrow X^2\Sigma^+$.

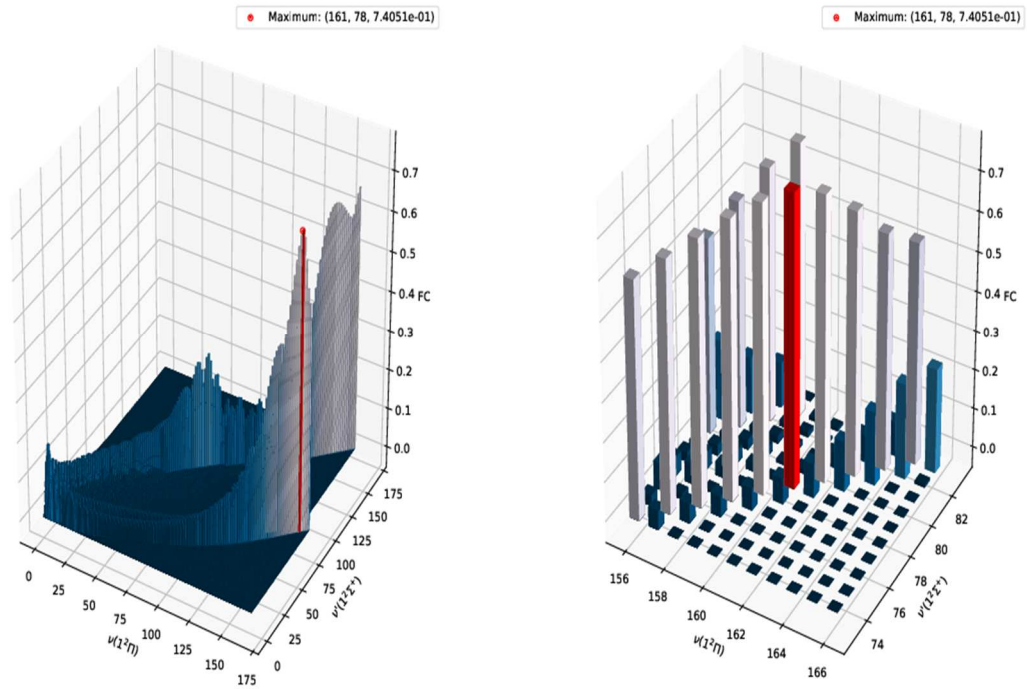

Figure 9: The calculated FCFs of RbBa for vibrational level of cooling transition $A^2\Pi \rightarrow X^2\Sigma^+$.